International Journal of Nanomedicine

Dovepress
open access to scientific and medical research

Open Access Full Text Article

ORIGINAL RESEARCH

Inhibition of proliferation and migration of tumor cells through phenylboronic acid-functionalized polyamidoamine-mediated delivery of a therapeutic DNAzyme Dz13

This article was published in the following Dove Press journal:
International Journal of Nanomedicine

Jiebing Yang*
Jiayuan Zhang*
Jiakai Xing
Zhiyuan Shi
Haobo Han
Quanshun Li

Key Laboratory for Molecular Enzymology and Engineering of Ministry of Education, School of Life Sciences, Jilin University, Changchun 130012, People's Republic of China

*These authors contributed equally to this work

Background: The phenylboronic acid-functionalized polyamidoamine (PP) was employed as a gene carrier for Dz13 delivery, inducing an obvious anticancer response.

Materials and methods: The Dz13 condensation ability of PP was evaluated through gel retardation assay. The cellular uptake mechanism of PP/Dz13 nanoparticles was studied using confocal laser scanning microscope and flow cytometer. The inhibition ability of cell proliferation, migration and invasion was investigated through MTT assay, flow cytometry, wound healing and Transwell migration assays, using hepatocarcinoma cell line HepG2 as a model. Finally, Western blotting analysis was used to detect the signaling pathway associated with the inhibition of cell apoptosis and migration induced by Dz13 delivery.

Results: The carrier PP could efficiently condense Dz13 into stable nanoparticles at mass ratios of >1.5. The hydrodynamic diameter and zeta potential of PP/Dz13 nanoparticles were measured to be 204.77 nm and +22.00 mV at a mass ratio of 10.0, respectively. The nanoparticles could realize an efficient cellular uptake in sialic acid-dependent endocytosis manner. Moreover, the nanoparticles exhibited an obvious antiproliferation effect through the induction of cell apoptosis and cell cycle arrest due to the cleavage of *c-Jun* mRNA. Besides, the suppression of cell migration and invasion could be achieved after the PP/Dz13 transfection, attributing to the decreased expression level of *MMP-2* and *MMP-9*.

Conclusion: The PP provided a potential delivery system to achieve the tumor-targeting gene therapy.

Keywords: phenylboronic acid, polyamidoamine, DNAzyme, gene therapy, antiproliferation effect, antimigration effect

Introduction

Cancer has been considered to be one of the leading causes of death, accounting for millions of deaths annually owing to the uncontrolled proliferation rate.[1–4] In the past three decades, extensive studies have confirmed that the genesis and development of malignant tumors were highly associated with the maladjustment of gene expression or regulation.[5,6] With the advantages in manipulating gene expression, gene therapy has emerged as an attractive approach to achieve the delivery of therapeutic genes to specific cells in cancer treatment.[7,8] Among the therapeutic strategies, deoxyribozymes (DNAzymes) are a new class of synthetic DNA molecules, which could specifically bind its target mRNA through the base-pairing mode

Correspondence: Haobo Han; Quanshun Li
Key Laboratory for Molecular Enzymology and Engineering of Ministry of Education, School of Life Sciences, Jilin University, Qianjin Street 2699, Changchun 130012, People's Republic of China
Tel +86 431 8515 5201
Fax +86 431 8515 5200
Email hanhb1310@mails.jlu.edu.cn; quanshun@jlu.edu.cn

submit your manuscript | www.dovepress.com
DovePress
http://doi.org/10.2147/IJN.S211744

and then realize the cleavage of mRNA.[9,10] As the most important member, the "10–23" subtype of DNAzyme exhibited a favorable catalytic activity to cleave the target mRNA between unpaired purine and paired pyrimidine through the de-esterification reaction.[11,12] Particularly, a therapeutic DNAzyme Dz13 targeting and cleaving the *c-Jun* mRNA has been demonstrated to significantly inhibit the tumor growth through the induction of caspase-2 activation.[13–17] Furthermore, Dz13 exhibited great antimetastasis efficacy by reducing the expression of matrix metalloproteinase (*MMP*)-2 and *MMP-9* in tumors.[13] Therefore, Dz13 is considered to be a potential candidate for realizing the tumor gene therapy. However, the clinical application of Dz13 is seriously hindered by the low stability and cellular uptake efficiency, and thus an efficient delivery system is highly required for facilitating the Dz13-based gene therapy.[18]

Synthetic carriers such as cationic polymers have been widely studied and considered to be promising alternatives to viral-based gene carriers in the field of gene delivery due to their low immunogenicity and favorable transfection efficiency.[19,20] Among the cationic polymers, an amine-terminated dendrimer polyamidoamine (PAMAM) has attracted great interest in the field of gene delivery owing to its superior properties such as well-defined structure, excellent biocompatibility and versatile modification owing to its multiple amine groups.[21–23] Positively charged PAMAM dendrimer could efficiently condense the nucleic acids into stable nanoparticles and facilitate their escape from endo/lysosomes through the "proton sponges" effect, eventually realizing efficient gene transfection.[24,25] Unfortunately, the transfection efficiency of PAMAM could not fulfill the therapeutic requirements, thereby limiting the clinic application in tumor gene therapy. Inspired by the surface engineering technology, the amine groups on the surface of PAMAM could be modified with various reagents to enhance the gene delivery efficiency such as fluoric anhydride,[26] nucleobase analog,[27,28] amino acids[29] and lactobionic acid.[30] Besides, the conjugation of targeting ligands on the PAMAM dendrimer was another attractive approach to improve the gene transfer based on the receptor-mediated endocytosis pathway.[31–33] As known, cancer proliferation and metastasis were closely related to the high expression of sialic acid, which has been proposed as an important biomarker in malignant tumors.[34,35] Meanwhile, phenylboronic acid (PBA) has been proved to be an efficient ligand which could specially recognize the sialic acid overexpressed in various types of malignant tumors, indicating that PBA could be employed as a potential motif for facilitating the tumor-targeting drug/gene delivery.[34–37]

In this study, the PBA-functionalized polyamidoamine (PP) was developed and employed as a carrier to realize the intracellular delivery of Dz13, as shown in Scheme 1. Following the successful transfection of PP/Dz13 nanoparticles, the inhibition of cell proliferation and migration was systematically investigated, using human hepatocarcinoma cell line HepG2 as a model.

Materials and methods

Materials

Dz13 (5′-CGGGAGGAAGGCTAGCTACAACGAGAGGC GTTG-3′), Dz13Scr as negative control (5′-GCGAC GTGAGGCTAGCTACAACGAGTGGAGGAG-3′), FAM-labeled Dz13 (Dz13-FAM) and Cy3-labeled Dz13 (Dz13-Cy3) were acquired from Sangon Biotech (Shanghai, China).

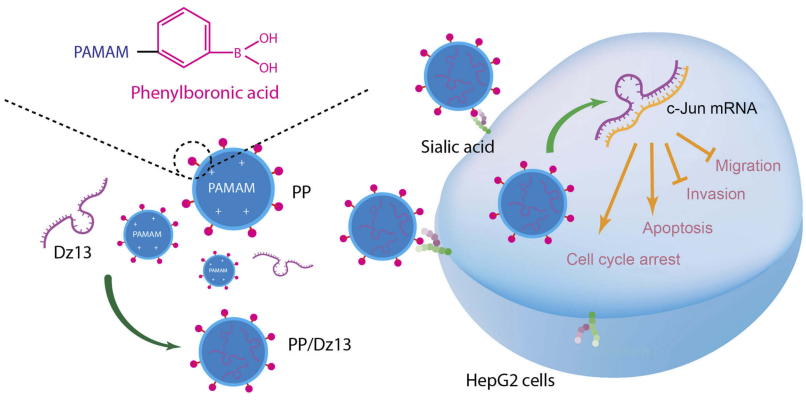

Scheme 1 The construction of phenylboronic acid-functionalized polyamidoamine (PP) and its application in Dz13 delivery.
Abbreviation: PAMAM, polyamidoamine.

The amine-terminated G5 PAMAM dendrimer was purchased from Chenyuan Co. (Weihai, China). 4-Carboxyphenylboronic acid, 1-[3-(dimethylamino)propyl]-3-ethyl carbodiimine (EDC) and N-hydroxysuccinimide (NHS) were obtained from Aladdin (Shanghai, China). DMEM and LIVE/DEAD® Viability/Cytotoxicity kit were provided by Thermo Fisher Scientific (Waltham, MA, USA). FBS was purchased from Kangyuan Co. (Beijing, China). The Annexin V-FITC/PI apoptosis detection kit was purchased from Vazyme Biotech (Nanjing, China). Cell cycle detection kit was purchased from BestBio (Shanghai, China). Bicinchoninic acid (BCA) protein assay kit was obtained from BioTeke (Beijing, China). The mitochondrial membrane potential assay kit was provided by Beyotime (Nanjing, China). MTT was obtained from Amersco, Inc. (Solon, OH, USA). Polyvinylidene fluoride (PVDF) membrane was purchased from Millipore (Billerica, MA, USA). Antibodies against c-Jun, procaspase-2, procaspase-3, procaspase-8, procaspase-9, p53, MMP-2, MMP-9, PARP and β-actin and horseradish peroxidase (HRP)-labeled goat anti-rabbit or anti-mouse secondary antibodies were purchased from Abcam (Shanghai, China). The human hepatocarcinoma cell line HepG2 and hepatocyte L02 were obtained from the Shanghai Institute of Cell Bank (Shanghai, China). All other reagents were used without further purification.

Synthesis and characterization of PP

Briefly, 4-carboxyphenylboronic acid (5.76 mg), EDC (39.90 mg) and NHS (23.96 mg) were dissolved in 1 mL methanol separately, and these solutions were mixed together. After stirring at room temperature for 4 hrs, PAMAM solution (100 mg PAMAM in 1 mL methanol) was added dropwise into the reaction system, and the mixture was stirred at room temperature for 24 hrs. Finally, the solution was dialyzed against distilled water for 48 hrs in a dialysis bag (MWCO: 3500 Da), and the product was obtained through lyophilization. The structure of PP was characterized by an AVANCE DMX 500 NMR spectrum (Bruker, Rheinstetten, Germany) using D_2O as the solvent. Transmission electron microscopy (TEM) images of PAMAM/Dz13 and PP/Dz13 nanoparticles were obtained using HITACHI-H800 microscope with an accelerating voltage of 100 kV. Scanning electron microscope (SEM) images of nanoparticles were captured on a JSM7900 field emission microscope (JEOL, Tokyo, Japan) with an accelerating voltage of 1 kV. The hydrodynamic diameter and zeta potential values of nanoparticles were tested by Nano ZS90 Zetasizer (Malvern, UK).

Gel retardation assay

The Dz13-binding ability of PP was estimated by agarose gel retardation. The nanoparticles were prepared by incubating PP and Dz13 with different mass ratios at 37°C for 30 mins and then loaded on 1% agarose gel electrophoresis in Tris-acetate–EDTA buffer at 80 V for 20 mins. To further confirm the protective effect of PP for Dz13, PP/Dz13 nanoparticles were treated with DNase I for 30 mins and 4 mg/mL of heparin sodium for 2 hrs, and then analyzed by agarose gel electrophoresis as described above. The bands were detected by a Tanon 1600 gel imaging system (Tanon, Shanghai, China).

Cellular uptake assay of PP/Dz13 nanoparticles

The HepG2 cells were inoculated in 6-well plates with 2 mL of 10% FBS-containing DMEM (density: 2.5×10^5 cells/well) and cultured at 37°C overnight. Then, the medium was discarded and the cells were incubated with PP/Dz13-FAM and PAMAM/Dz13-FAM nanoparticles at different mass ratios for 6 hrs (5 μg/mL Dz13-FAM for each group). The cells were collected and assayed to obtain the optimal mass ratio for Dz13 transfection by BD FACS caliber (BD Bioscience Mountain View, Franklin Lakes, NJ, USA). Further, the intracellular uptake of PP/Dz13-FAM nanoparticles was detected through confocal laser scanning microscopy (CLSM). Briefly, the cells were inoculated in 6-well plates with a sterilized coverslip in each well (density: 2.0×10^5 cells/well) and cultured in 2 mL of 10% FBS-containing DMEM for 24 hrs. After the pretreatment with 1 mM PBA for 1 hr, the cells were incubated with PP/Dz13-FAM (mass ratio of 10.0) and PAMAM/Dz13-FAM nanoparticles (mass ratio of 7.5) in serum-free medium for 6 hrs, harboring 5 μg/mL Dz13-FAM in each group. After washing with PBS twice, the cells were fixed with 75% ethanol and the nuclei were stained with DAPI solution at a final concentration of 1 μg/mL, and the coverslip was detected using LSM 710 confocal laser scanning microscope (Carl Zeiss Microscopy LLC, Jena, Germany). In addition, the intracellular uptake mechanism of PP/Dz13 nanoparticles was studied through flow cytometry as follows: the cell culture and the PBA pretreatment were conducted as described above, and then the cells were treated with PP/Dz13-Cy3 (mass ratio of 10.0) and PAMAM/Dz13-Cy3 nanoparticles (mass ratio of 7.5) harboring 5 μg/mL Dz13-Cy3 in serum-free medium for 6 hrs, and the harvested cells were detected by BD FACS caliber (BD Bioscience Mountain View).

Endosomal escape analysis of PP/Dz13 nanoparticles

The HepG2 cells were seeded in 6-well plates with sterilized coverslips at an initial density of 2.5×10^5 cells/well and cultured at 37°C overnight. Then, the cells were treated with 1 mL serum-free DMEM harboring PP/Dz13-FAM nanoparticles for 2, 6 and 10 hrs (mass ratio of 10.0, 5 μg/mL Dz13-FAM), respectively. After staining with LysoTracker Red (ThermoFisher, Eugene, OR, USA) for 5 mins, 4% paraformaldehyde solution was used to fix the cells which were dyed with DAPI solution (1 μg/mL) for 5 mins. Finally, the coverslips were analyzed on a LSM 710 confocal laser scanning microscope (Carl Zeiss Microscopy LLC, Jena, Germany) to detect the endosomal escape of PP/Dz13 nanoparticles.

Inhibition of cell proliferation assay

The cells were seeded in 96-well plates at a density of 8.0×10^3 cells/well and incubated at 37°C overnight. Then, the cells were incubated with PP and PAMAM of different concentrations for 48 hrs in the carrier cytotoxicity assay, or incubated with PAMAM/Dz13 and PP/Dz13 nanoparticles in serum-free DMEM for 6 hrs (mass ratios of 7.5 and 10.0, respectively) and in 10% FBS-containing DMEM for 48 hrs in the antiproliferative assay. Subsequently, 20 μL of MTT solution (5 mg/mL) was added into each well, and the plates were kept at 37°C for 4 hrs. After the addition of 200 μL dimethyl sulfoxide (DMSO) to dissolve the formed formazan crystal, the cell viability was calculated as the ratio of the optical density values at 520 nm of treated cells and untreated cells, which were detected using HBS-1096A microplate reader (Detie, Nanjing, China).

Live/dead cell staining

The HepG2 cells were inoculated in 6-well plates at a density of 2.5×10^5 cells/well and cultured at 37°C overnight. Then, the cells were treated with PP/Dz13 (mass ratio of 10.0) and PAMAM/Dz13 nanoparticles (mass ratio of 7.5) containing 5 μg/mL Dz13 in serum-free medium for 6 hrs and further in 10% FBS-containing DMEM for 48 hrs. Based on the manufacturer's instructions, live/dead reagents were used to stain the cells which were observed by Olympus IX73P1F fluorescence microscopy (Tokyo, Japan).

Inhibition of colony formation assay

The cell culture and the treatment with PP/Dz13 or PAMAM/Dz13 nanoparticles were conducted as described in section "Live/dead cell staining". The treated cells were harvested and reseeded into disparate wells of 6-well plates at a density of 2.0×10^4 cells/well and incubated at 37°C for 7 days. The cells were fixed with cold 75% ethanol at 4°C for 20 mins and stained with 0.2% crystal violet solution for an additional 15 mins. Finally, the colony formation was observed by Olympus IX73P1F fluorescence microscopy.

Cell apoptosis and cell cycle arrest analysis

The HepG2 cells were seeded into 6-well plates at a density of 2.0×10^5 cells/well and incubated at 37°C for 24 hrs. Then, the cells were treated with PP/Dz13 or PAMAM/Dz13 nanoparticles (mass ratios of 10.0 and 7.5, respectively) containing 5 μg/mL Dz13 in serum-free medium for 6 hrs and incubated in 10% FBS-containing DMEM for 72 hrs. For the cell apoptosis analysis, the treated cells were dyed with Annexin V-FITC and PI staining solution according to the manufacture's protocol and detected by CytoFLEX flow cytometer (Beckman Coulter Inc., USA). For the cell cycle arrest analysis, the transfected cells were fixed with cold 75% ethanol at −20 °C for 1 hr and then treated with PI/RNase staining buffer for 15 mins based on the manufacturer's protocol, and finally the cells were detected and analyzed on a BD FACS caliber (BD Bioscience Mountain View), using the BD CellQuest Pro software for analysis.

Western blotting analysis

The cell culture and treatment were performed as described in the section "Cell apoptosis and cell cycle arrest analysis". The cells were harvested, washed with PBS and lysed in the RIPA buffer containing 1 mM phenylmethanesulfonyl fluoride on ice for 15 mins. The cell lysis solutions were centrifuged at 12,000 rpm for 15 mins to collect the supernatants. Total protein concentration of each sample was quantified by BCA protein assay kit. Equal amount of proteins was applied in 12% SDS-PAGE and transferred to PVDF membrane by electroblotting. The membrane was first blocked with 5% skim milk at room temperature for 2 hrs and incubated with the corresponding primary antibodies at 4°C overnight. After washing with PBS containing 0.1% Tween (PBST) for 10

mins three times, the membrane was treated with HRP-labeled secondary antibody at room temperature for 1 hr and washed with PBST for 10 mins three times. Finally, the expression level of targeted proteins was detected by enhanced chemiluminescence on a Tanon 2500 chemiluminescence imaging system (Tanon).

Mitochondrial membrane potential assay

The mitochondrial membrane potential was measured using the lipophilic JC-1 dye. The cell culture and treatment were carried out as described in the section "Cell apoptosis and cell cycle arrest analysis". Briefly, the harvested cells were washed with PBS three times, stained with JC-1 dye at 37°C for 30 mins, and observed with Olympus IX73P1F fluorescence microscopy after washing with PBS another three times. The ratio of red to green fluorescence was measured using Image J software.

Wound healing analysis

The HepG2 cells were seeded in 6-well plates at a density of 1.0×10^6 cells/well and incubated at 37°C until the confluence of cells reached 90%. Then, a scratched wound in the monolayer of cells was generated using a 200-μL sterile pipette tip. After washing with PBS twice, the cells were cultured with different nanoparticles as described in the section "Cell apoptosis and cell cycle arrest analysis". Following the incubation for 12, 24, 36 and 48 hrs, the length of wounds was imaged with Olympus IX73P1F fluorescence microscopy and the anti-migration function of Dz13 transfection was evaluated.

Transwell migration analysis

The treatment of HepG2 cells was performed as described in section "Inhibition of colony formation assay", and the Transwell migration analysis was carried out using a Transwell chamber. The serum-free DMEM (200 μL) containing 2.0×10^4 transfected cells and 1% BSA was added into the upper chamber, and meanwhile 700 μL DMEM was added into the lower chamber. Following the incubation at 37°C for 24 hrs, the nonmigrating cells on the top of membrane were removed by mechanical wiping, and the ones migrating to the lower surface of membrane were fixed with 75% ethanol at 4°C for 20 mins. After the staining with 0.1% crystal violet solution for 15 mins, the cells were washed with PBS three times and detected on an Olympus IX73P1F fluorescence microscopy.

Statistical analysis

All the data were presented as mean value ± SD, and the statistical significance of differences between experimental groups and control group was calculated using one-way ANOVA with GraphPad Prism 6 complemented with Student's *t*-test (n.s., not significant; $*p<0.05$; $**p<0.01$ and $***p<0.001$).

Results and discussion

Construction and characterization of PP/Dz13 nanoparticles

According to the synthetic procedure in Figure 1A, the tumor-targeting carrier PP was constructed through the EDC/NHS-mediated conjugation of ligand PBA with the amine groups on the surface of PAMAM dendrimer. The structure of product PP was identified using ^{1}H NMR (Figure 2). Clearly, the proton peaks at 7.55 and 7.46 ppm generated from the aromatic ring of PBA indicated the successful modification of PBA on the surface of PAMAM. Based on the measurement of boron content by an inductively coupled plasma optical emission spectrometer, the conjugation ratio of PBA on the surface of PP was calculated to be 7.2 as reported in our previous research.[37] Then, the Dz13-binding and condensation ability of PP was evaluated through gel retardation assay (Figure 1B). Compared with free Dz13, the carriers PAMAM and PP could realize the complete retardation of Dz13 when the mass ratios were higher than 1.5, indicating that Dz13 could be condensed into stable nanoparticles via electrostatic interaction. The critical mass ratio of PP was the same as that of PAMAM which meant that the modification with ligand PBA did not alter the binding and condensation ability with Dz13. Meanwhile, the protective effect of PP for Dz13 against DNase degradation was detected through agarose gel electrophoresis, in which PP/Dz13 and DNase I were coincubated and subsequently treated with heparin to obtain free Dz13. As shown in Figure S1, clear Dz13 band could be observed when PP/Dz13 nanoparticles were subjected to DNase I and subsequent heparin treatment, revealing that the presence of PP could effectively protect Dz13 from the degradation of DNase. The improved stability against enzymes will be beneficial for the stable and efficient delivery of nanoparticles, especially at an in vivo level.

Further, the morphology of PP/Dz13 and PAMAM/Dz13 nanoparticles was characterized by TEM and SEM. As shown in Figure 3, PP/Dz13 and PAMAM/Dz13

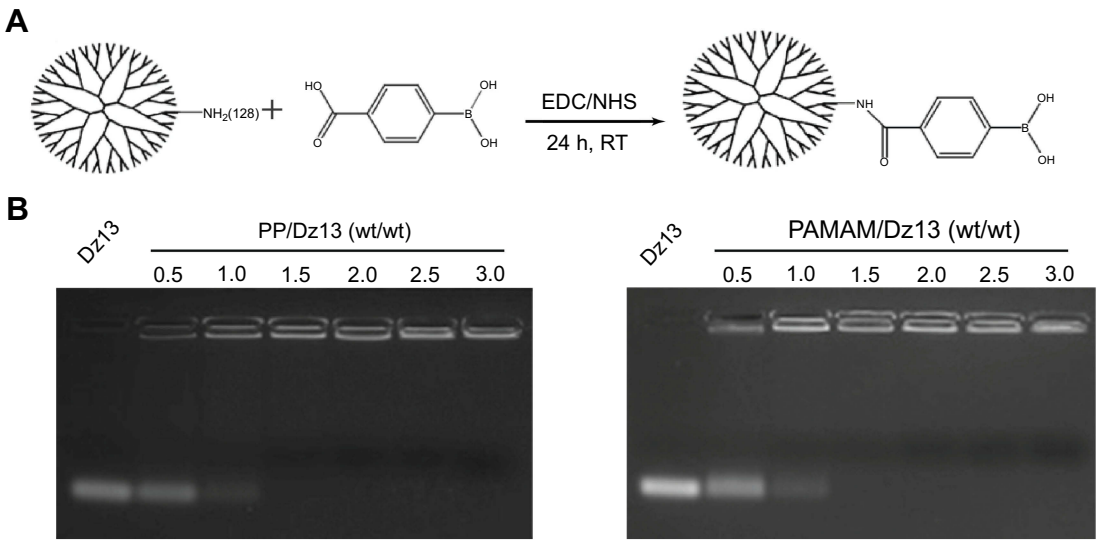

Figure 1 (**A**) The synthetic illustration of the gene carrier PP and (**B**) gel retardation assay for the Dz13 binding and condensation ability of PP and PAMAM.
Abbreviations: PP, phenylboronic acid-functionalized polyamidoamine; PAMAM, polyamidoamine; EDC/NHS, 1-[3-(dimethylamino)propyl]-3-ethyl carbodiimine/N-hydroxysuccinimide; RT, room temperature.

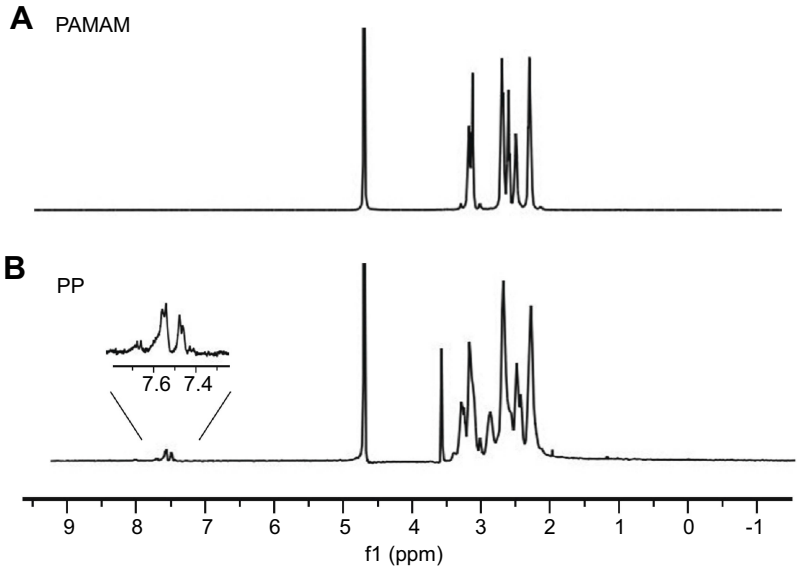

Figure 2 The ^{1}H NMR spectra of (**A**) PAMAM and (**B**) PP in D_2O.
Abbreviations: PP, phenylboronic acid-functionalized polyamidoamine; PAMAM, polyamidoamine.

nanoparticles possessed a similar spherical structure with the size of approximately 200 nm. SEM images also showed the spherical structure with a smooth surface for both the PP/Dz13 and PAMAM/Dz13 nanoparticles, and the particle size of these two nanoparticles was observed to be ca. 200 nm (Figure S2). The hydrodynamic diameter and zeta potential values of nanoparticles at different mass ratios were determined through Malvern Nano ZS90 Zetasizer (Table S1). Apparently, the hydrodynamic diameter values decreased with the increasing mass ratio of carrier to Dz13 for these two groups, suggesting the successful formation of nanoparticles. The zeta potential values exhibited an increasing tendency with the improved ratio of cationic polymers. The particle size and zeta potential values of PP/Dz13 nanoparticles were determined to be 204.77 nm and +22.00 mV at a mass ratio of 10.0, respectively, which was the optimal ratio for Dz13 transfection as introduced in the following studies. The

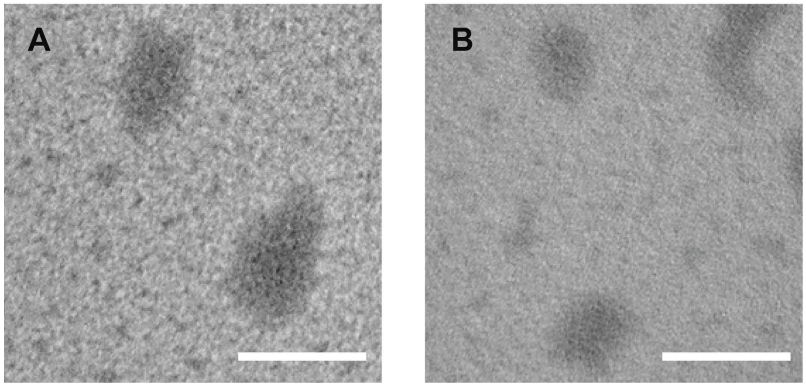

Figure 3 The TEM images of PAMAM/Dz13 (**A**) and PP/Dz13 nanoparticles (**B**). The scale bar is 200 nm.
Abbreviations: PP, phenylboronic acid-functionalized polyamidoamine; PAMAM, polyamidoamine.

favorable particle size (ca. 200 nm) and positively charged state of nanoparticles provided excellent properties for facilitating the intracellular uptake and gene transfection of nanoparticles.

Intracellular distribution of PP/Dz13 nanoparticles

To determine the optimal mass ratio of carrier and Dz13 for intracellular delivery, the transfection efficiency of nanoparticles containing FAM-labeled Dz13 was investigated through flow cytometry. As shown in Figure S3, compared with free Dz13, stronger green fluorescence could be detected in carrier-mediated Dz13 transfections at different mass ratios, indicating that both PAMAM and PP could efficiently enhance the intracellular delivery of Dz13. In particular, the highest transfection efficiency of PP/Dz13 and PAMAM/Dz13 nanoparticles could be achieved at mass ratios of 10.0 and 7.5, respectively, which was highly relied on their desirable particle size and positive charge on the surface. The transfection efficiency of PP/Dz13 nanoparticles at the mass ratio of 10.0 was measured to be 88.0%. Thus, these two ratios were employed as the optimal mass ratio of PP/Dz13 and PAMAM/Dz13 nanoparticles in the subsequent studies.

As PBA has been widely reported to specifically recognize the sialic acid overexpressed on the surface of tumor cells,[34–37] the intracellular uptake behavior of PP/Dz13 nanoparticles was analyzed using CLSM and flow cytometry. As demonstrated in Figure 4, compared with the PAMAM-mediated Dz13 delivery, stronger fluorescence could be observed in the PP/Dz13 transfection, indicating that PP could enhance the intracellular delivery of Dz13 due to the introduction of the tumor-targeted ligand PBA molecules. Interestingly, the fluorescence intensity could be significantly reduced in the PP/Dz13 transfection group when HepG2 cells were pretreated with 1 mM PBA for 1 hr, whereas obvious green fluorescence could be detected in the PAMAM/Dz13 group regardless of the pretreatment of PBA molecules. The results indicated that the excessive PBA possessed an inhibitory effect on the PP-mediated Dz13 transfection. The results were probably caused by the fact that free PBA could shield the sialic acids expressed on the membrane of HepG2 cells and further prevent the endocytosis of PP/Dz13 nanoparticles. Thus, we could conclude that the PP-mediated delivery of Dz13 relied on the sialic acid-dependent endocytosis in HepG2 cells. In contrast, the pretreatment of PBA did not induce the inhibition of endocytosis of PP/Dz13 nanoparticles in human hepatocyte L02 (Figure S4), which was demonstrated to exhibit lower expression level of sialic acids.[33] Consistently, the pretreatment of PBA did not alter the cellular uptake performance of PAMAM/Dz13 nanoparticles in flow cytometric analysis, whereas significant inhibition of endocytosis could be obtained in PP/Dz13 transfection group when HepG2 cells were preincubated with 1 mM PBA (Figure S5A). Meanwhile, the pretreatment of PBA did not change the endocytotic behavior of PP/Dz13 and PAMAM/Dz13 nanoparticles in L02 cells (Figure S5B). In summary, compared with free PAMAM, the introduction of PBA on the surface of PAMAM could enhance the intracellular delivery of Dz13, which was achieved in a sialic acid-dependent endocytosis manner.

Finally, the endosomal escape of PP/Dz13 nanoparticles was investigated using CLSM (Figure 5). At 2 and 6 hrs, obvious colocation of green and red fluorescence could be observed, suggesting that PP/Dz13 nanoparticles

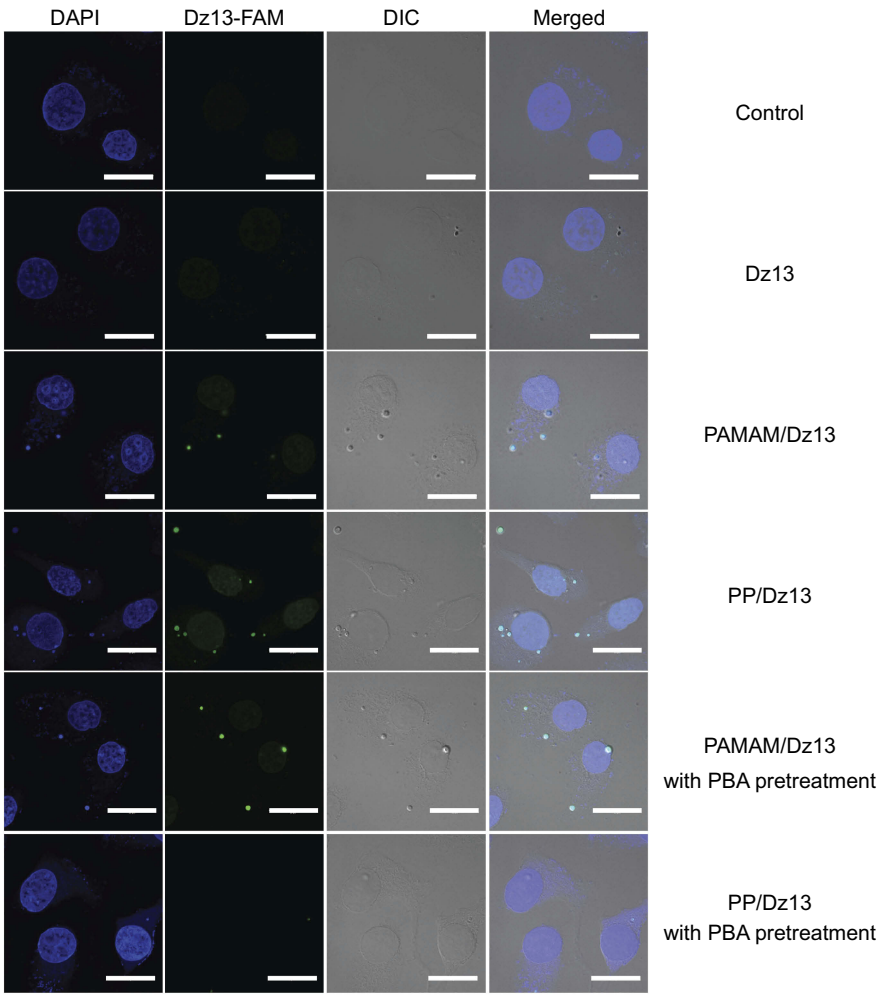

Figure 4 The CLSM images of HepG2 cells transfected with PP/Dz13 and PAMAM/Dz13 nanoparticles with the pretreatment of 1 mM PBA for 1 hr. The scale bar is 20 μm.
Abbreviations: CLSM, confocal laser scanning microscopy; PP, phenylboronic acid-functionalized polyamidoamine; PAMAM, polyamidoamine.

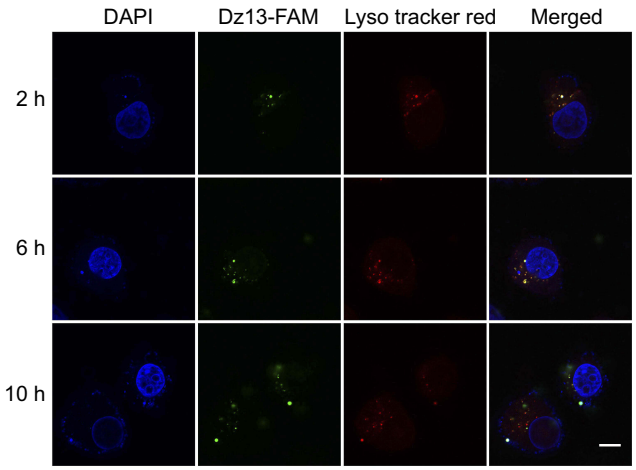

Figure 5 Endosomal escape of PP/Dz13 nanoparticles through CLSM. The scale bar is 10 μm.
Abbreviations: CLSM, confocal laser scanning microscopy; PP, phenylboronic acid-functionalized polyamidoamine; PAMAM, polyamidoamine.

were mainly located in the lysosomes. Notably, green fluorescence could be observed in the cytosol after 10 hrs, not merged with red fluorescence. Thus, it could be concluded that PP/Dz13 nanoparticles achieved an efficient endosomal escape owing to the "proton sponge" effect, which would facilitate the release of Dz13 to executive its antitumor function.

Inhibition of cell proliferation by PP/Dz13 nanoparticles

Before the antiproliferative analysis of PP/Dz13 nanoparticles, the cytotoxicity of PP and PAMAM was evaluated using HepG2 and L02 cells. As shown in Figure S6, in comparison to HepG2 cells, PAMAM exhibited higher cytotoxicity against L02 cells at an identical concentration since normal cells were more sensitive than cancer cells.

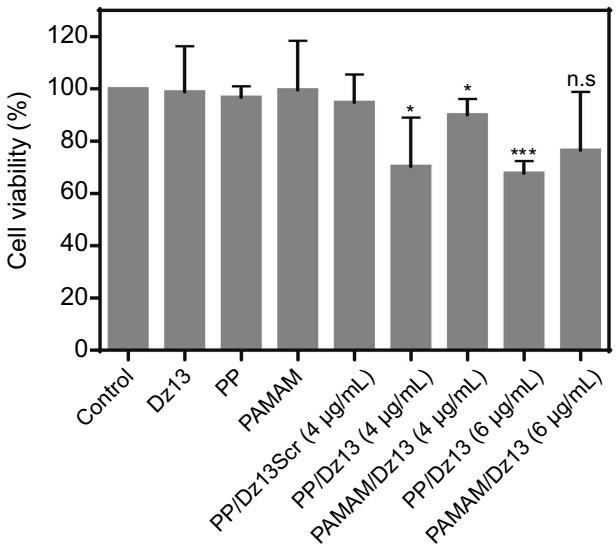

Figure 6 The inhibition of cell proliferation in HepG2 cells after the transfection of PP/Dz13 (mass ratio of 10) and PAMAM/Dz13 nanoparticles (mass ratio of 7.5). The concentrations of free PP and PAMAM were 40 and 30 μg/mL, respectively. The data were presented as mean value ± SD of triplicate measurements (n.s., not significant; *p<0.05 and ***p<0.001).
Abbreviations: PP, phenylboronic acid-functionalized polyamidoamine; PAMAM, polyamidoamine.

However, the derivative PP showed lower cytotoxicity than PAMAM in these two cell lines, especially for L02 cells at a high concentration of carriers (100 μg/mL). The reduced cytotoxicity was mainly caused by the reduction of positively charged amine groups on the surface of PAMAM. Then, the cell viability of HepG2 cells after the carrier-mediated Dz13 transfection was detected through MTT method (Figure 6). Apparently, compared with the control group, there was no inhibition of cell proliferation obtained in the PP/Dz13Scr group, whereas the carrier-mediated Dz13 transfection possessed an obvious inhibitory effect on the proliferation of tumor cells owing to the carrier-mediated successful delivery of therapeutic Dz13. Specifically, the PP-mediated Dz13 delivery exhibited higher inhibition efficiency than PAMAM/Dz13 groups, with cell viability values of 70.4% and 67.8% at the Dz13 concentration of 4 and 6 μg/mL, respectively. The favorable inhibition of cell proliferation was also an indicator of the superior transfection efficiency of PP. Based on the cell viability analysis after the PP-mediated Dz13 delivery (mass ratio of 10.0), IC_{50} of Dz13 was calculated to be 15.38 μg/mL (Figure S7). Moreover, a larger population of dead cells could be clearly observed in PP/Dz13 nanoparticles group through live/dead cell staining, where the viable cells emitted the green fluorescence and the dead cells generated red

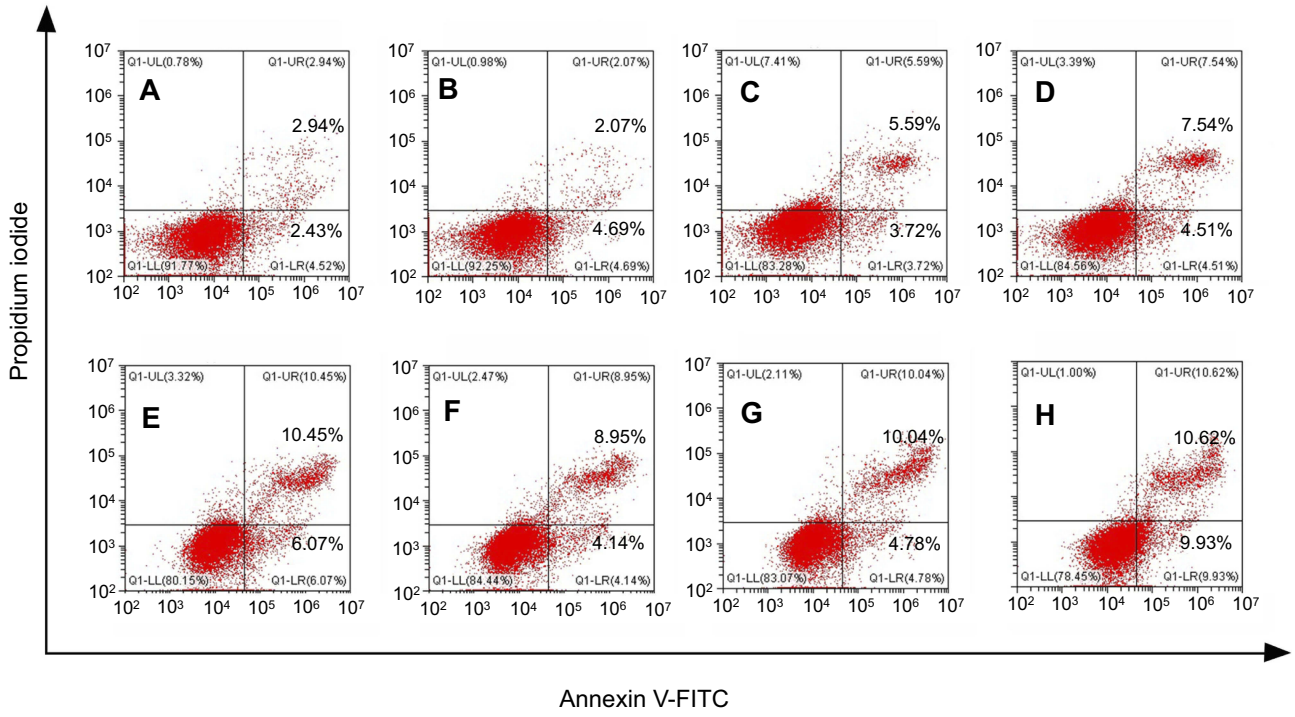

Figure 7 The cell apoptosis analysis of HepG2 cells after the transfection of PP/Dz13 and PAMAM/Dz13 nanoparticles: (**A**) control, (**B**) Dz13, (**C**) PP, (**D**) PP/Dz13Scr, (**E**) PAMAM/Dz13, (**F**) PAMAM, (**G**) PAMAM/Dz13Scr and (**H**) PP/Dz13 nanoparticles.
Abbreviations: PP, phenylboronic acid-functionalized polyamidoamine; PAMAM, polyamidoamine.

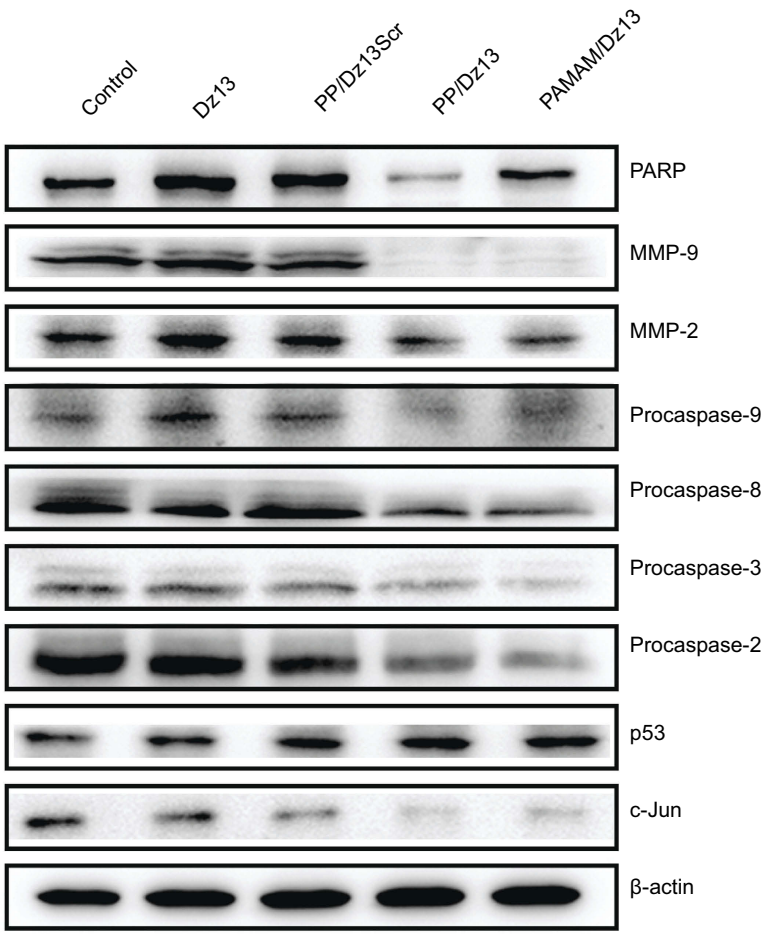

Figure 8 Western blotting assay for the expression level of associated proteins in HepG2 cells after Dz13 transfection.
Abbreviations: PP, phenylboronic acid-functionalized polyamidoamine; PAMAM, polyamidoamine.

fluorescence (Figure S8). Consistently, PP/Dz13 nanoparticles could remarkably inhibit the cell colony formation, much stronger than PP/Dz13Scr group (Figure S9). In summary, these results illustrated that the carrier-mediated Dz13 transfection could efficiently inhibit the cell proliferation due to the tumor-suppressive function of Dz13 and PP/Dz13 exhibited higher inhibition ability due to the enhanced transfection efficiency.

Subsequently, the cell apoptosis induced by Dz13 transfection was evaluated by Annexin V-FITC/PI staining followed by flow cytometric analysis. As shown in Figure 7, compared with the control group, limited early apoptosis could be observed in the PAMAM/Dz13Scr and PP/Dz13Scr groups, but enhanced ratio of late apoptosis could be clearly obtained for these two groups. These results were probably caused by the certain cleavage ability of Dz13Scr on the *c-jun* mRNA, though the sequence was scrambled. In contrast, PP/Dz13 and PAMAM/Dz13 nanoparticles exhibited a higher percentage of early and late apoptosis, with the total ratios of 20.55% and 16.52%, respectively, revealing that Dz13 transfection-mediated by PAMAM and PP could efficiently facilitate the cell apoptosis. In addition, lower apoptosis ratio was achieved in free PP than PAMAM, indicating the lower cytotoxicity of PP, and the results were consistent with MTT assay. To further elaborate the apoptosis pathways induced by Dz13 delivery, the expression level of apoptosis-associated proteins was determined through Western blotting. As shown in Figure 8, PP/Dz13 and PAMAM/Dz13 nanoparticles could significantly reduce the expression of *procaspase-3* and promote the conversion of procaspase-3 to caspase-3, which has been identified as a key mediator of apoptosis in mammalian cells.[38] Meanwhile, the expression level of poly(ADP-ribose) polymerase (*PARP*) was decreased after the treatment with PP/Dz13 and PAMAM/Dz13 nanoparticles, which was triggered by the cleavage of caspases-3. Additionally, the expression levels

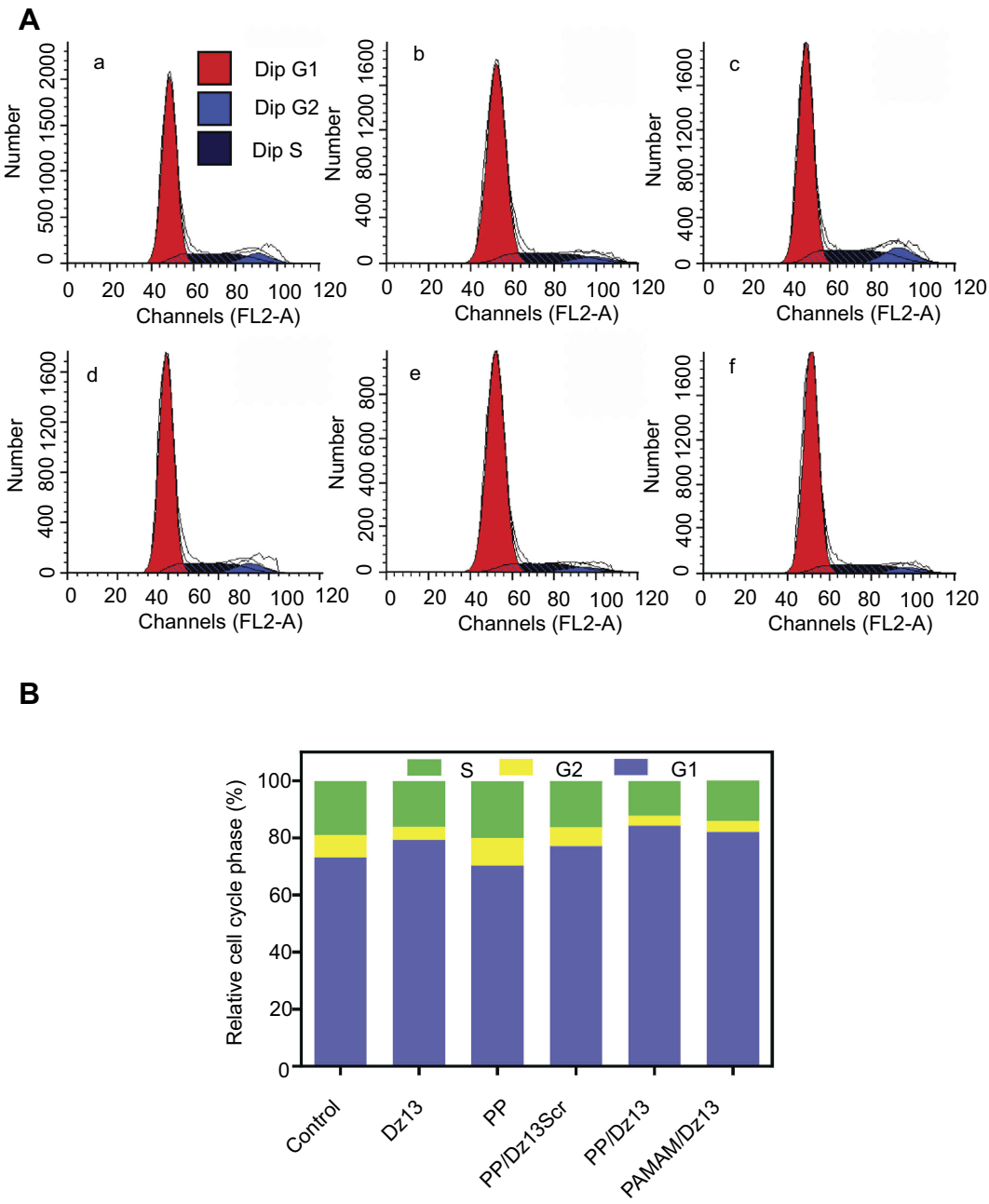

Figure 9 Cell cycle arrest (**A**) and the relative cell cycle phase (**B**) in HepG2 cells after Dz13 transfection: (a) control, (b) Dz13, (c) PP, (d) PP/Dz13Scr, (e) PP/Dz13 and (f) PAMAM/Dz13 nanoparticles.

Abbreviations: PP, phenylboronic acid-functionalized polyamidoamine; PAMAM, polyamidoamine.

of *procaspase-8* and −*9* decreased after the carriers-mediated Dz13 transfection, suggesting the activation of caspase-8 and −9 through the cleavage of their precursors. Basically, the activation of caspase-8 has been identified to play a critical role in the cell apoptosis through the death receptor-dependent pathway, while caspase-9 could initiate the cell apoptosis based on the mitochondria-dependent apoptotic pathway.[39,40] Thus, we inferred that the carrier-mediated Dz13 transfection could trigger the cell apoptosis through both death receptor-dependent pathway and mitochondrial apoptotic signaling pathway. The mitochondrial membrane potential was detected after the Dz13 transfection using lipophilic JC-1 probe to further demonstrate the activation of mitochondrial apoptotic pathway. As shown in Figure S10 and S11, compared with the control group, a stronger green fluorescence generated from the monomer state of JC-1 could be observed in the PP/Dz13 and PAMAM/Dz13 groups, indicating that Dz13 transfection could reduce the

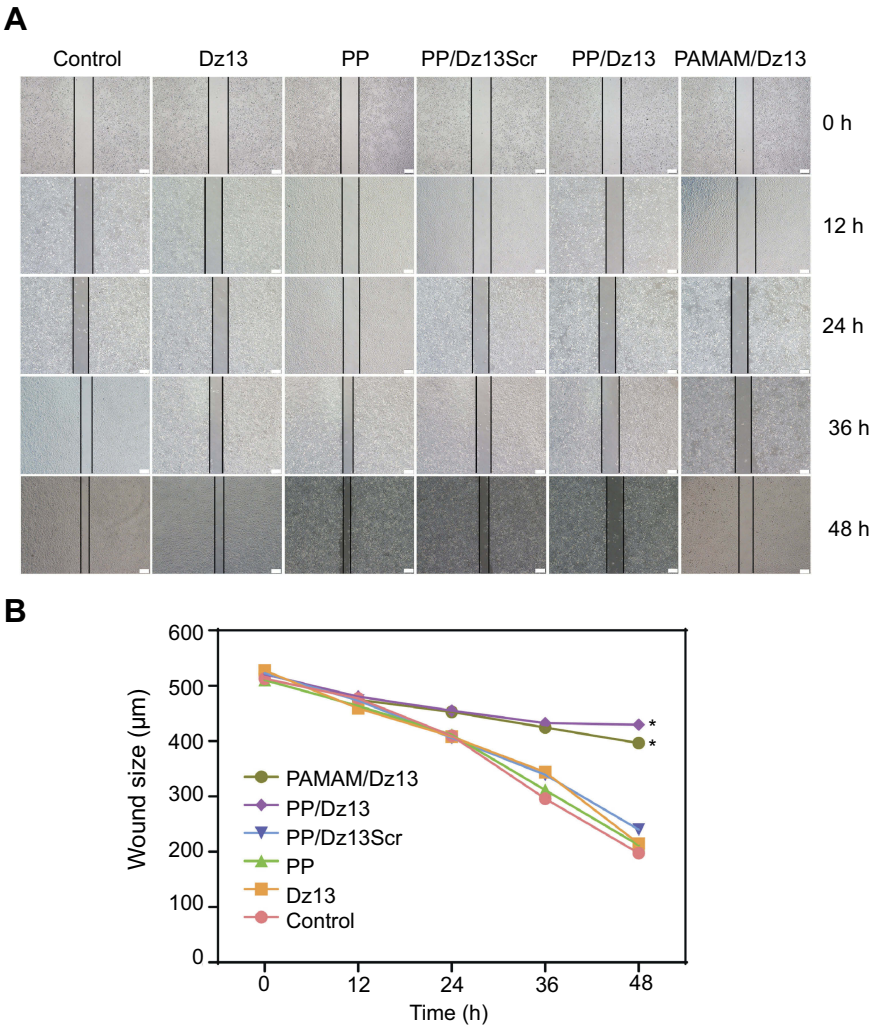

Figure 10 The antimigration assay in HepG2 cells after Dz13 transfection for different incubation times (**A**) and the quantitative wound size (**B**). The data were presented as mean value ± SD of triplicate experiments (*p<0.05). The scale bar is 200 μm.
Abbreviations: PP, phenylboronic acid-functionalized polyamidoamine; PAMAM, polyamidoamine.

membrane potential of mitochondria. Consistently, the results also supported that the Dz13 delivery could trigger the cell apoptosis through the activation of mitochondria-dependent apoptotic pathway.

Further, the expression level of related proteins after Dz13 transfection was detected using Western blotting (Figure 8). Dz13 has been reported to target and cleave the *c-Jun* mRNA, and thus we detected the expression level of c-Jun protein. As expected, the expression of *c-Jun* was dramatically inhibited after the carrier-mediated Dz13 delivery. c-Jun protein, making up the transcription factor AP-1, has been confirmed to participate in the cell activities such as proliferation, transformation and apoptosis.[13] Thus, the downregulation of c-Jun protein could trigger the cell apoptosis. Meanwhile, Dz13 transfection could reduce the expression of *procaspase-2*, indicating the activation of caspase-2 which could induce the mitochondrial permeability as Dz13 is known as a potent inducer of caspase-2.[14] Furthermore, the enhanced expression of p53 protein could be detected after the carrier-mediated Dz13 transfection, promoting the cell apoptosis through the p53-dependent route. As the activation of p53 was highly associated with the cell cycle arrest, the cell cycle arrest was detected after Dz13 transfection based on the PI staining and subsequent flow cytometric analysis. As shown in Figure 9, the cell proportion of G1 phase could be significantly improved following the treatment with PP/Dz13 and PAMAM/Dz13 nanoparticles, owing to the activation of *caspase-2* and upregulation of *p53*. These results revealed that the carrier-mediated Dz13

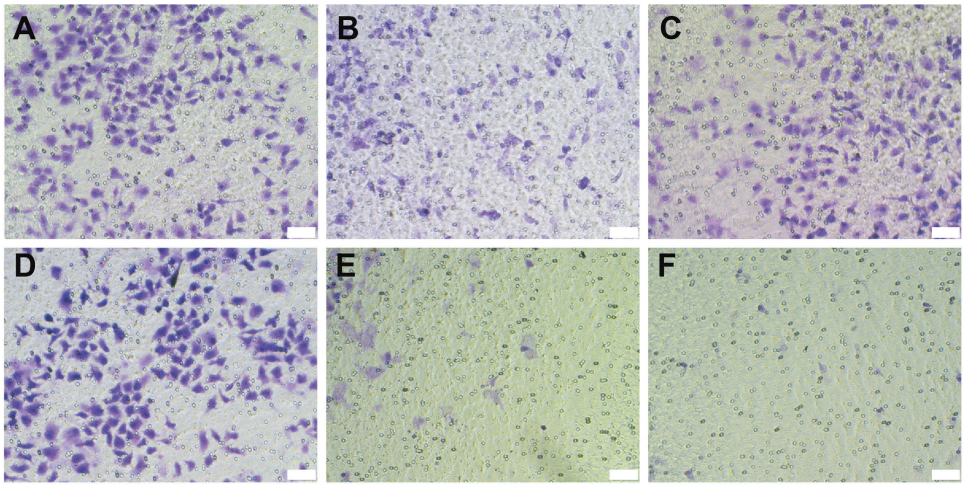

Figure 11 Transwell migration assay of HepG2 cells after the carriers-mediated Dz13 transfection: (**A**) control, (**B**) Dz13, (**C**) PP, (**D**) PP/Dz13Scr, (**E**) PP/Dz13 and (**F**) PAMAM/Dz13 nanoparticles. The scale bar is 50 μm.
Abbreviations: PP, phenylboronic acid-functionalized polyamidoamine; PAMAM, polyamidoamine.

delivery could induce the cell cycle arrest at G1 phase contributing to the antiproliferative effect, except for the induction of cell apoptosis.

Inhibition of cell migration by PP/Dz13 nanoparticles

The metastasis has been identified to be one of the major causes of cancer death in patients, and thus it was necessary to determine the ability of Dz13 transfection to inhibit the cell migration and invasion. In the wound healing assay, the wound size of different groups exhibited an obvious decreased tendency with the elongation of incubation time (Figure 10). Notably, in comparison to the constant migration of control group, the cells treated with PP/Dz13 and PAMAM/Dz13 nanoparticles showed a strong inhibitory effect on the migration efficiency. Additionally, the invasive ability of HepG2 cells was tested following the Dz13 transfection through Transwell migration assay (Figure 11). Compared with the control and PP/Dz13Scr groups, the invasive cell number was sharply decreased for the cells treated with PAMAM/Dz13 and PP/Dz13 nanoparticles. All these results demonstrated that the carrier-mediated Dz13 delivery could efficiently inhibit cell migration and invasion. Since the cancer metastasis was usually associated with the extracellular MMPs secreted by the cancer cells,[41] the expression level of *MMP-2* and *−9* was further measured after Dz13 transfection. As shown in Figure 8, the expression level of *MMP-2* and *−9* was downregulated after the transfection of PAMAM/Dz13 and PP/Dz13 nanoparticles, indicating that the Dz13 transfection could achieve the inhibition of metastasis through the reduced expression of *MMP-2* and *−9*.

Conclusion

In conclusion, a tumor-targeting PAMAM derivative was successfully developed through the modification of ligand PBA on the surface of PAMAM dendrimer, and meanwhile, it was employed as an efficient delivery system of therapeutic DNAzyme Dz13. Compared with PAMAM, the derivative PP exhibited superior transfection efficiency owing to the sialic acid-dependent endocytosis pathway. Remarkably, PP/Dz13 nanoparticles could be capable of inhibiting the cell proliferation, migration and invasion through the cleavage of *c-Jun* mRNA in cancer cells. Overall, the PBA-functionalized PAMAM dendrimer provided an efficient platform for the delivery of therapeutic genes, thereby facilitating the cancer gene therapy in future clinical use.

Acknowledgment

The authors gratefully acknowledge the supports from National Key R&D Program of China (2018YFC1105401), National Natural Science Foundation of China (81673502 and 81872928), Province-University Cooperation Project of Jilin Province (SXGJQY2017-4), Science & Technology Department of Jilin Province (20190201288JC), Education Department of Jilin Province (JJKH20190010KJ) and Graduate Innovation Program of Jilin University (101832-01820).

Disclosure

The authors report no conflicts of interest in this work.

References

1. Kankala RK, Liu CG, Chen AZ, et al. Overcoming multidrug resistance through the synergistic effects of hierarchical pH-sensitive, ROS-generating nanoreactors. *ACS Biomater Sci Eng*. 2017;3:2431–2442. doi:10.1021/acsbiomaterials.7b00569
2. Chen BQ, Kankala RK, He GY, et al. Supercritical fluid-assisted fabrication of indocyanine green-encapsulated silk fibroin nanoparticles for dual-triggered cancer therapy. *ACS Biomater Sci Eng*. 2018;4:3487–3497. doi:10.1021/acsbiomaterials.8b00705
3. Xu PY, Kankala RK, Pan YJ, et al. Overcoming multidrug resistance through inhalable siRNA nanoparticles-decorated porous microparticles based on supercritical fluid technology. *Int J Nanomed*. 2018;13:4685–4698. doi:10.2147/IJN.S169399
4. Liu CG, Han YH, Zhang JT, et al. Rerouting engineered metal-dependent shapes of mesoporous silica nanocontainers to biodegradable Janus-type (sphero-ellipsoid) nanoreactors for chemodynamic therapy. *Chem Eng J*. 2019;370:1188–1199. doi:10.1016/j.cej.2019.03.272
5. Vile RG, Russell SJ, Lemoine N. Cancer gene therapy: hard lessons and new courses. *Gene Ther*. 2000;7:2–8. doi:10.1038/sj.gt.3301084
6. Lin S, Gregory RI. MicroRNA biogenesis pathways in cancer. *Nat Rev Cancer*. 2015;15:321–333. doi:10.1038/nrc3932
7. Naldini L. Gene therapy returns to centre stage. *Nature*. 2015;526:351–360. doi:10.1038/nature15818
8. Wirth T, Parker N, Yla-Herttuala S. History of gene therapy. *Gene*. 2013;525:162–169. doi:10.1016/j.gene.2013.03.137
9. Wu P, Hwang K, Lan T, et al. A DNAzyme-gold nanoparticle probe for uranyl ion in living cells. *J Am Chem Soc*. 2013;135:5254–5257. doi:10.1021/ja400150v
10. Liu H, Yu X, Chen Y, et al. Crystal structure of an RNA-cleaving DNAzyme. *Nat Commun*. 2017;8:2006. doi:10.1038/s41467-017-02203-x
11. Khachigian LM. Deoxyribozymes as catalytic nanotherapeutic agents. *Cancer Res*. 2019;79:879–888. doi:10.1158/0008-5472.CAN-18-2474
12. Xing Z, Gao S, Duan Y, et al. Delivery of DNAzyme targeting aurora kinase A to inhibit the proliferation and migration of human prostate cancer. *Int J Nanomed*. 2015;10:5715–5727. doi:10.2147/IJN.S90559.
13. Elahy M, Dass CR. Dz13: c-Jun downregulation and tumour cell death. *Chem Biol Drug Des*. 2011;78:909–912. doi:10.1111/j.1747-0285.2011.01166.x.
14. Kim SH, Dass CR. Induction of caspase-2 activation by a DNA enzyme evokes tumor cell apoptosis. *DNA Cell Biol*. 2012;31:1–7. doi:10.1089/dna.2011.1323
15. Dass CR, Galloway SJ, Choong PF. Dz13, a c-jun DNAzyme, is a potent inducer of caspase-2 activation. *Oligonucleotides*. 2010;20:137–146. doi:10.1089/oli.2009.0226
16. Meng L, Ma W, Lin S, et al. Tetrahedral DNA nanostructure-delivered DNAzyme for gene silencing to suppress cell growth. *ACS Appl Mater Interfaces*. 2019;11:6850–6857. doi:10.1021/acsami.8b22444
17. Eicher AC, Dobler D, Kiselmann C, et al. Dermal delivery of therapeutic DNAzymes via chitosan hydrogels. *Int J Pharm*. 2019. doi:10.1016/j.ijpharm.2019.04.005
18. Pouton CW, Seymour LW. Key issues in non-viral gene delivery. *Adv Drug Deliv Rev*. 2001;46:187–203. doi:10.1016/S0169-409X(00)00133-2
19. El-Aneed A. An overview of current delivery systems in cancer gene therapy. *J Control Release*. 2004;94:1–14. doi:10.1016/j.jconrel.2003.09.013
20. Zhang J, Wu D, Xing Z, et al. N-Isopropylacrylamide-modified polyethylenimine-mediated p53 gene delivery to prevent the proliferation of cancer cells. *Colloids Surf B Biointerfaces*. 2015;129:54–62. doi:10.1016/j.colsurfb.2015.03.032
21. Lee CC, MacKay JA, Frechet JM, et al. Designing dendrimers for biological applications. *Nat Biotechnol*. 2005;23:1517–1526. doi:10.1038/nbt1171
22. Majoros IJ, Myc A, Thomas T, et al. PAMAM dendrimer-based multifunctional conjugate for cancer therapy: synthesis, characterization, and functionality. *Biomacromolecules*. 2006;7:572–579. doi:10.1021/bm0506142
23. Han H, Chen W, Yang J, et al. 2-Amino-6-chloropurine-modified polyamidoamine-mediated p53 gene transfection to achieve antitumor efficacy. *New J Chem*. 2018;42:13375–13381. doi:10.1039/C8NJ01870G
24. Zhou J, Wu J, Hafdi N, et al. PAMAM dendrimers for efficient siRNA delivery and potent gene silencing. *Chem Commun*. 2006;22:2362–2364. doi:10.1039/b601381c
25. Wang M, Cheng Y. The effect of fluorination on the transfection efficacy of surface-engineered dendrimers. *Biomaterials*. 2014;35:6603–6613. doi:10.1016/j.biomaterials.2014.04.065
26. Wang M, Liu H, Li L, et al. A fluorinated dendrimer achieves excellent gene transfection efficacy at extremely low nitrogen to phosphorus ratios. *Nat Commun*. 2014;5:3053. doi:10.1038/ncomms5972
27. Wang H, Wei H, Huang Q, et al. Nucleobase-modified dendrimers as nonviral vectors for efficient and low cytotoxic gene delivery. *Colloids Surf B Biointerfaces*. 2015;136:1148–1155. doi:10.1016/j.colsurfb.2015.11.015
28. Han H, Yang J, Wang Y, et al. Nucleobase-modified polyamidoamine-mediated miR-23b delivery to inhibit the proliferation and migration of lung cancer. *Biomater Sci*. 2017;5:2268–2275. doi:10.1039/c7bm00599g
29. Choi JS, Nam K, Park JY, et al. Enhanced transfection efficiency of PAMAM dendrimer by surface modification with L-arginine. *J Control Release*. 2004;99:445–456. doi:10.1016/j.jconrel.2004.07.027
30. Iacobazzi RM, Porcelli L, Lopedota AA, et al. Targeting human liver cancer cells with lactobionic acid-G (4)-PAMAM-FITC sorafenib loaded dendrimers. *Int J Pharm*. 2017;528:485–497. doi:10.1016/j.ijpharm.2017.06.049
31. Chen W, Liu Y, Liang X, et al. Chondroitin sulfate-functionalized polyamidoamine as a tumor-targeted carrier for miR-34a delivery. *Acta Biomater*. 2017;57:238–250. doi:10.1016/j.actbio.2017.05.030
32. Jiang LY, Lv B, Luo Y. The effects of an RGD-PAMAM dendrimer conjugate in 3D spheroid culture on cell proliferation, expression and aggregation. *Biomaterials*. 2013;34:2665–2673. doi:10.1016/j.biomaterials.2013.01.003
33. Wu D, Yang J, Xing Z, et al. Phenylboronic acid-functionalized polyamidoamine-mediated Bcl-2 siRNA delivery for inhibiting the cell proliferation. *Colloids Surf B Biointerfaces*. 2016;146:318–325. doi:10.1016/j.colsurfb.2016.06.034
34. Deshayes S, Cabral H, Ishii T, et al. Phenylboronic acid-installed polymeric micelles for targeting sialylated epitopes in solid tumors. *J Am Chem Soc*. 2013;135:15501–15507. doi:10.1021/ja406406h
35. Matsumoto A, Cabral H, Sato N, et al. Assessment of tumor metastasis by the direct determination of cell-membrane sialic acid expression. *Angew Chem Int Ed*. 2010;49:5494–5497. doi:10.1002/anie.201001220
36. Song Z, Liang X, Wang Y, et al. Phenylboronic acid-functionalized polyamidoamine-mediated miR-34a delivery for the treatment of gastric cancer. *Biomater Sci*. 2019;7:1632–1642. doi:10.1039/c8bm01385c
37. Yang J, Zhang J, Liu Y, et al. Phenylboronic acid-modified polyamidoamine-mediated delivery of short GC rich DNA for hepatocarcinoma gene therapy. *Biomater Sci*. 2019;7:3348–3358. doi:10.1039/C9BM00394K
38. Yang TJ, Haimovitz-Friedman A, Verheij M. Anticancer therapy and apoptosis imaging. *Exp Oncol*. 2012;34:269–276.
39. Dong M, Chen J, Zhang J, et al. A chemoenzymatically synthesized cholesterol-*g*-poly(amine-*co*-ester)-mediated p53 gene delivery for achieving antitumor efficacy in prostate cancer. *Int J Nanomed*. 2019;14:1149–1161. doi:10.2147/IJN.S191905

40. Wang Y, Li H, Li Y, et al. Identification of natural compounds targeting Annexin A2 with an anti-cancer effect. *Protein Cell*. 2018;9:568–579. doi:10.1007/s13238-018-0513-z

41. Tan ML, Choong PF, Dass CR. Direct anti-metastatic efficacy by the DNA enzyme Dz13 and downregulated MMP-2, MMP-9 and MT1-MMP in tumours. *Cancer Cell Int*. 2010;10:9. doi:10.1186/1475-2867-10-9